Active sites-rich zeolitic imidazolate framework/MXene heterostructure modified separator with improved Li^+ transport for high-performance Li-S batteries

Leiping Liao [a], Huanhuan Duan [a], Guohua Chen [b], Yuanfu Deng [a, c, *]

[a] The Key Laboratory of Fuel Cell for Guangdong Province, School of Chemistry and Chemical Engineering, South China University of Technology, Guangzhou 510640, PR China

[b] School of Energy and Environment, City University of Hong Kong, Tat Chee Avenue, Kowloon, Hong Kong SAR, China.

[c] Guangdong Provincial Research Center of Electrochemical Energy Engineering, South China University of Technology, Guangzhou 510640, PR China

Corresponding author: chyfdeng@scut.edu.cn.

1. Experimental section

1.1. Materials

MAX (Ti_3AlC_2) was bought from Jilin 11 Technology Co., Ltd. Hydrochloric acid (HCl) was purchased from Guangzhou Chemical Reagent Factory. Lithium fluoride (LiF) and 1-methyl-2-pyrrolidone (NMP) solvent were obtained from Shanghai Macklin Biochemical Co., ltd. Cobalt nitrate hexahydrate ($Co(NO_3)_2{\cdot}6H_2O$), 2-Methylimidazole, 1, 2-dimethoxyethane (DME), and 1, 3-dioxolane (DOL) were supplied by Aladdin Reagent Co., ltd. Polyvinylidene difluoride (PVDF) and lithium foils were received from Guangdong Canrd New Energy Technology Co., ltd. Sublimed sulfur (S) was purchased from Tianjin Kemiou Chemical Reagent Co., ltd. All chemicals were used directly without further purification.

1.2. Characterizations

The morphology and structure of the samples were characterized by a scanning electron

microscope (SEM, Merlin) and transmission electron microscope (TEM, JEM 2100F). The specific surface area and pore size distribution of the samples were investigated by a Micrometitics surface analyser (ASAP 2460) at 77 K. X-ray diffraction (XRD) was performed on a D8 Advance Powder Diffractometer. X-ray photoelectron spectroscopy (XPS, Kratos Axis Supra+) was employed to analyze the surface chemical compositions of the samples. The electrolyte contact angle of the modified separators was obtained with a Dataphysics OCA40 Micro. Ultraviolet–visible spectroscopy measurement was tested on a SHIMADZU UV-2600 spectrometer. The content of sulfur in KB/S was collected from a thermal gravimetric analyzer (TGA, TGA 550).

1.3. Visualized Adsorption of Polysulfides

2 mM Li_2S_6 solution was obtained by dissolving S and Li_2S (molar ratio of 5:1) into the solution of DME/DOL with a volume ratio of 1:1, and then stirring at 60 ℃ for 12 hours in an argon-filled glovebox. 20 mg of MXene and ZIF-L/MXene were added into 2 mL Li_2S_6 solution for comparison, respectively.

1.4. Assembly of Li_2S_6 symmetric batteries

Symmetric batteries were assembled with two identical ZIF-L/MXene or MXene electrodes, a Celgard 2500 separator, and 40 μL of Li_2S_6 electrolyte. The electrodes with a mass loading of 0.3 mg cm^{-2} were prepared by loading the homogeneous slurry of ZIF-L/MXene and PVDF in a weight ratio of 9:1 onto carbon-coated Al foils (circular disks with a diameter of 14 mm), followed by vacuum drying. For comparisons, the MXene electrodes were prepared by the same method. 0.2 M Li_2S_6 electrolyte was obtained by dissolving S and Li_2S (molar ratio of 5:1) into electrolyte which containing 1.0 M lithium bis (trifluoromethanesulfonyl) imide (LiTFSI) with 2 wt% $LiNO_3$ in DME/DOL (volume ratio of 1:1). The CV curves of the symmetric batteries were collected from a CHI660D electrochemical workstation at scan rates of 10 and 1000 mV s^{-1} between a voltage range of -1.5 to 1.5 V.

1.5. Cathode preparation and electrochemical tests

S and KB powder were mixed in ethanol with stirring for 40 min and dried at 60 °C. Then,

the KB/S composite was obtained through a melt-diffusion process with heat treatment at 210 °C for 12 h in an argon (Ar) atmosphere. The TGA curve shown in Supplementary Figure 3 suggested that the sulfur content in the KB/S composite is 75.5%. The as-prepared KB/S composite and PVDF were stirred in NMP with a mass ratio of 9:1 to obtain a homogeneous slurry. Subsequently, the aforesaid slurry was coated on carbon-coated Al foils (circular disks with a diameter of 14 mm) and dried under vacuum at 60 °C for later use. The S mass loadings of regular cathodes were between 1.2-1.5 $mg \cdot cm^{-2}$ and the high loading was up to ~ 4.1 $mg \cdot cm^{-2}$.

The electrochemical performances were carried out by using CR2016-type coin cells, and the cells were assembled in an Ar-filled glove box. Pure lithium metal and ZIF-L/MXene@PP MXene@PP were used as the anodes and separators, respectively. 1.0 M LiTFSI dissolved in DME/DOL (volume ratio of 1:1) with 2 wt% $LiNO_3$ additive as electrolyte. The ratio of electrolyte/S was 20 $\mu L \cdot mg^{-1}$ for the ordinary electrodes and 10 $\mu L \cdot mg^{-1}$ for the high sulfur loading electrodes. The GCD tests were measured on a multichannel battery test system (Neware CT-3008W) with a voltage range from 1.7 to 2.8 V. CV measurements were performed on an electrochemical workstation (CHI660D), and the EIS was tested from 0.01 Hz to 100 kHz.

2. Supplementary figures and tables

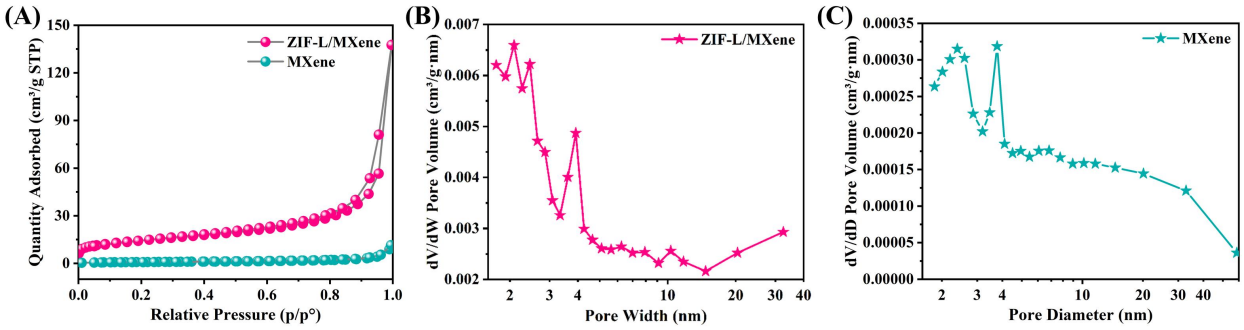

Supplementary Figure 1. (A) N_2 adsorption-desorption isotherms of the MXene and ZIF-L/MXene. The pore distribution curves of the (B) ZIF-L/MXene and (C) MXene.

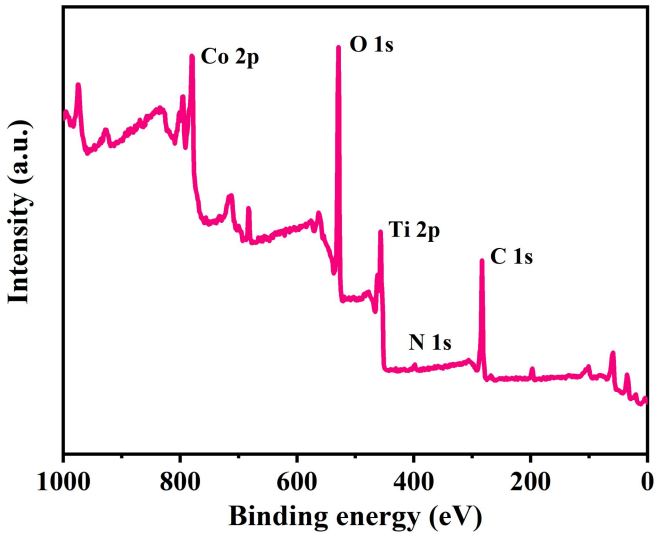

Supplementary Figure 2. XPS survey spectrum of the ZIF-L/MXene.

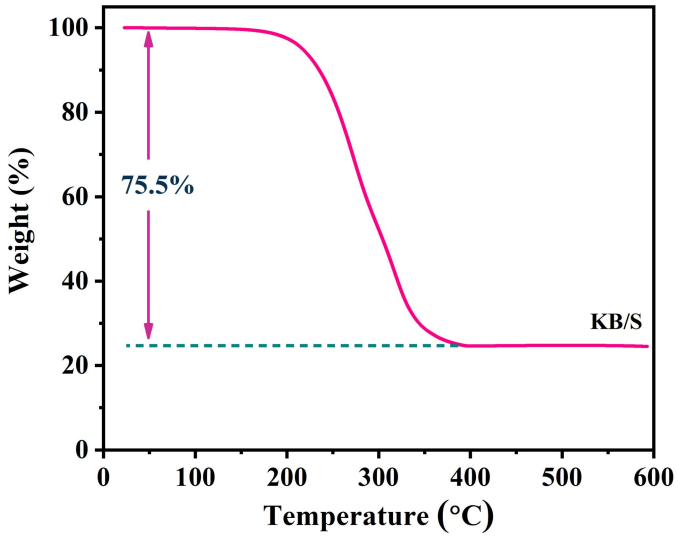

Supplementary Figure 3. TGA curve of the KB/S at N_2 atmosphere.

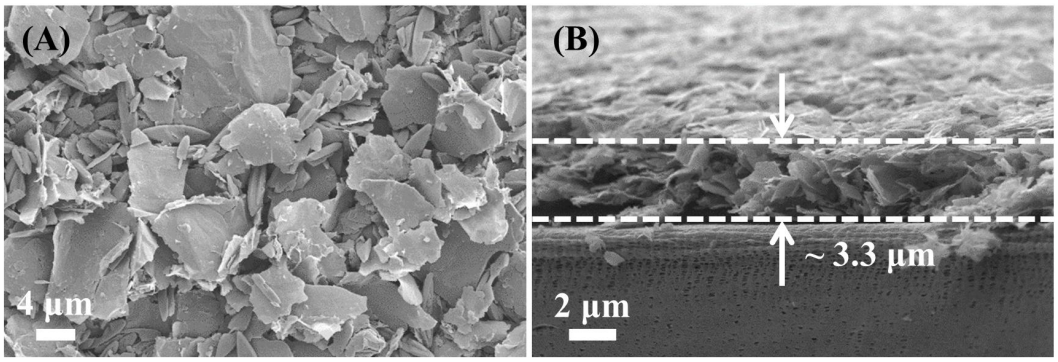

Supplementary Figure 4. (A) SEM and (B) Cross-sectional SEM images of the ZIF-L/MXene@PP separator.

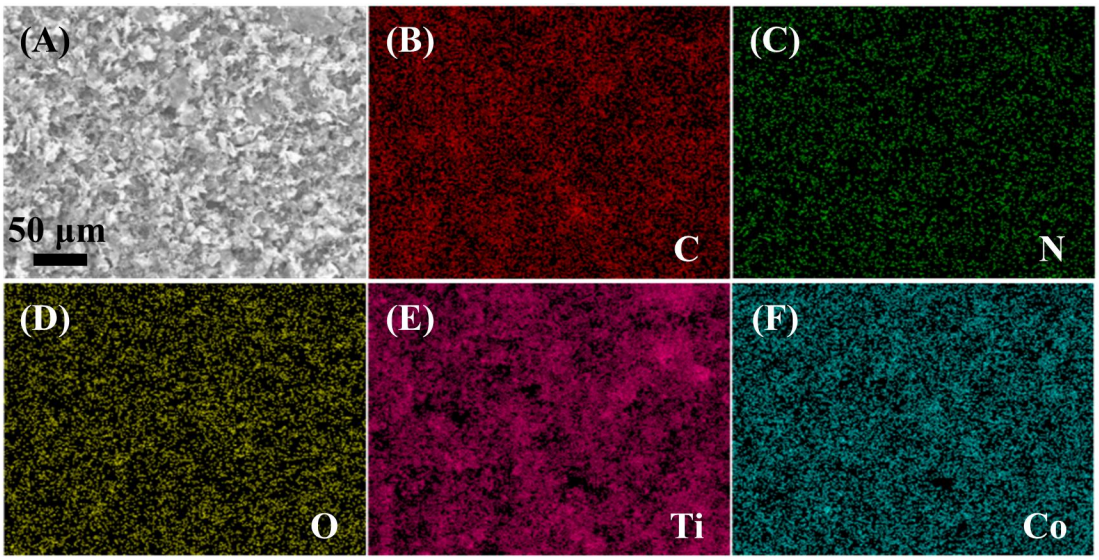

Supplementary Figure 5. (A) SEM and (B-F) the corresponding element mapping images of the ZIF-L/MXene@PP separator.

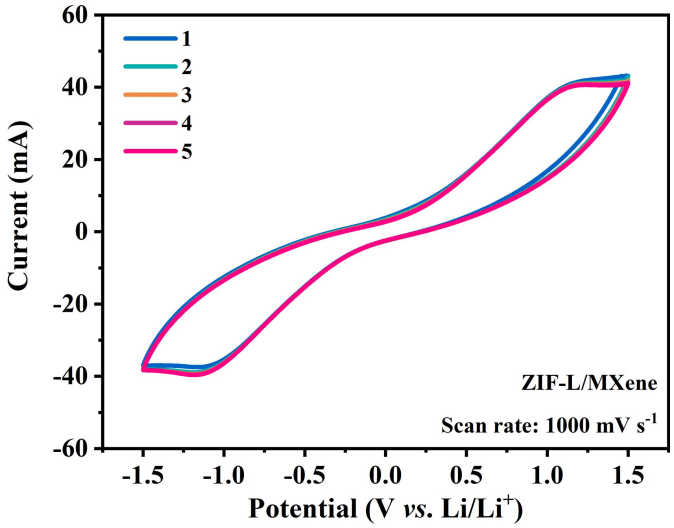

Supplementary Figure 6. CV curves of the ZIF-L/MXene-based symmetric cell at 1000 mV s^{-1}.

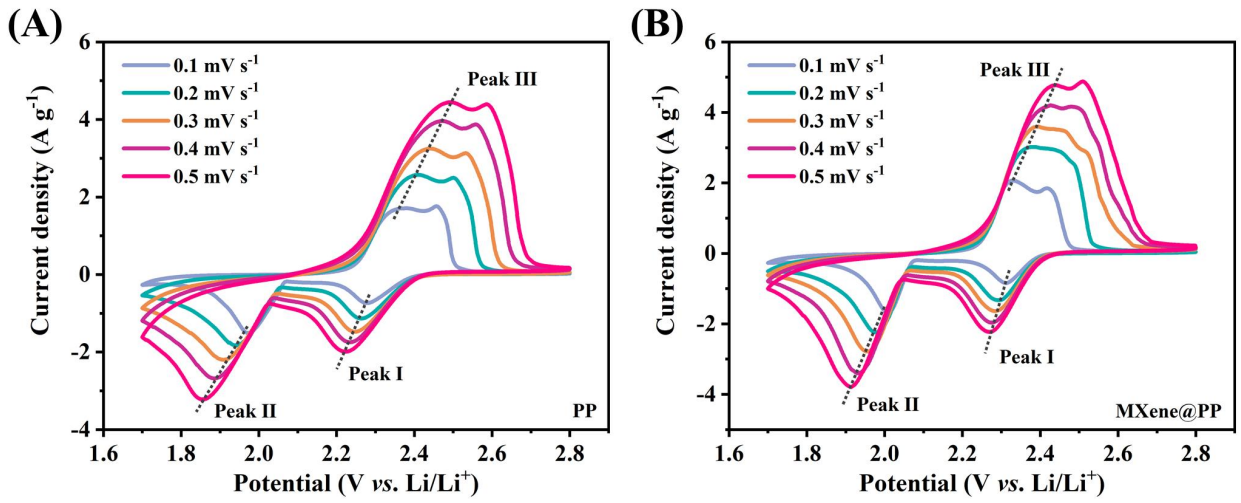

Supplementary Figure 7. CV curves of the (A) PP-based and (B) MXene@PP-based symmetric cells at different scan rates.

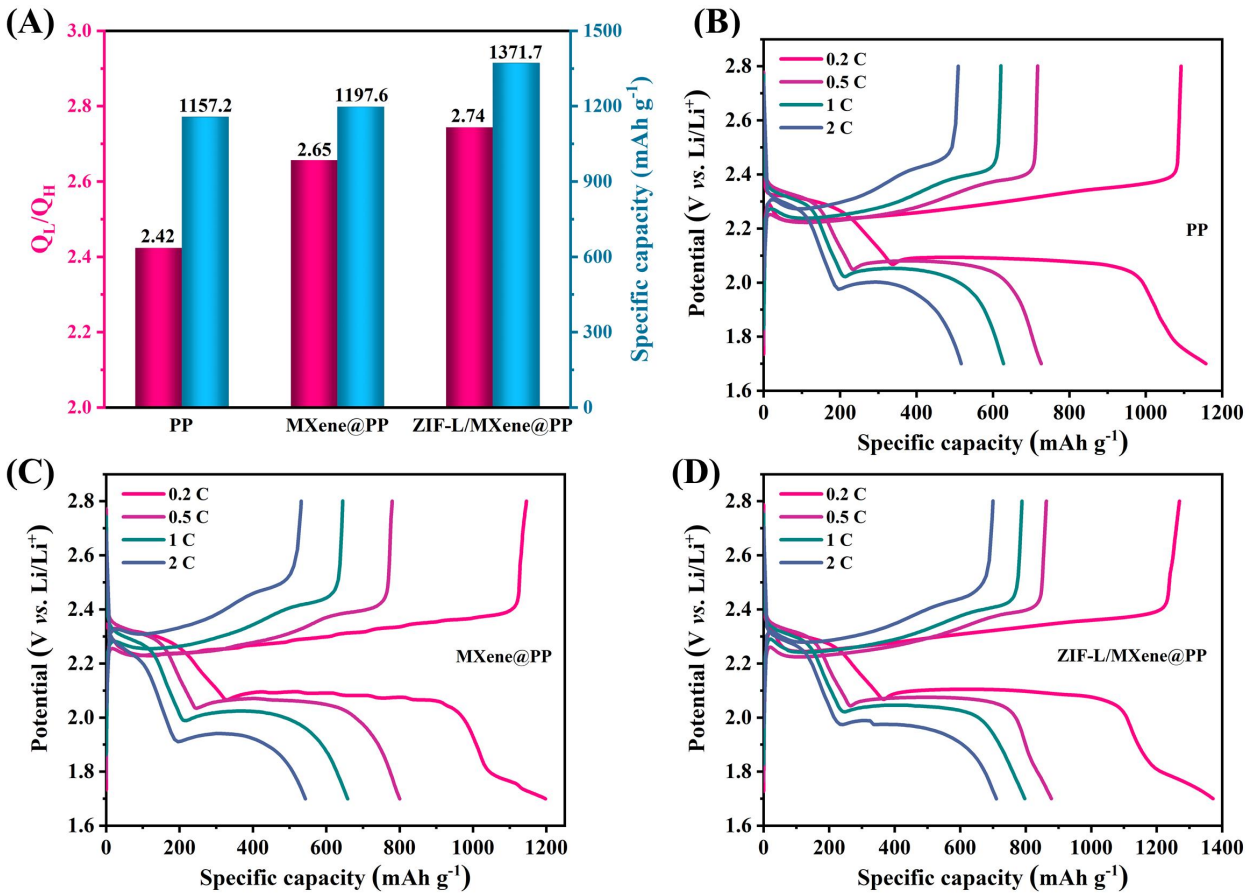

Supplementary Figure 8. (A) Q_L/Q_H and specific capacities of the PP, MXene@PP, and ZIF-L/MXene@PP-based Li-S cells, respectively. The charge–discharge curves of the (B) PP, (C) MXene@PP, and (D) ZIF-L/MXene@PP-based Li-S cells at different rates, respectively.

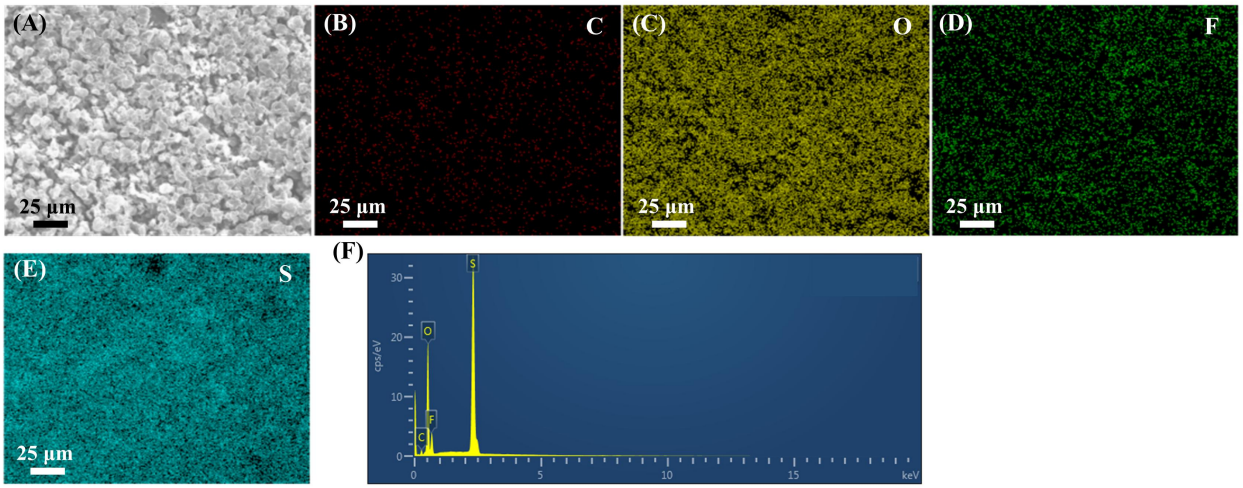

Supplementary Figure 9. (A) SEM image and (B-F) corresponding element analysis of Li metal anode from the PP-based Li-S cell.

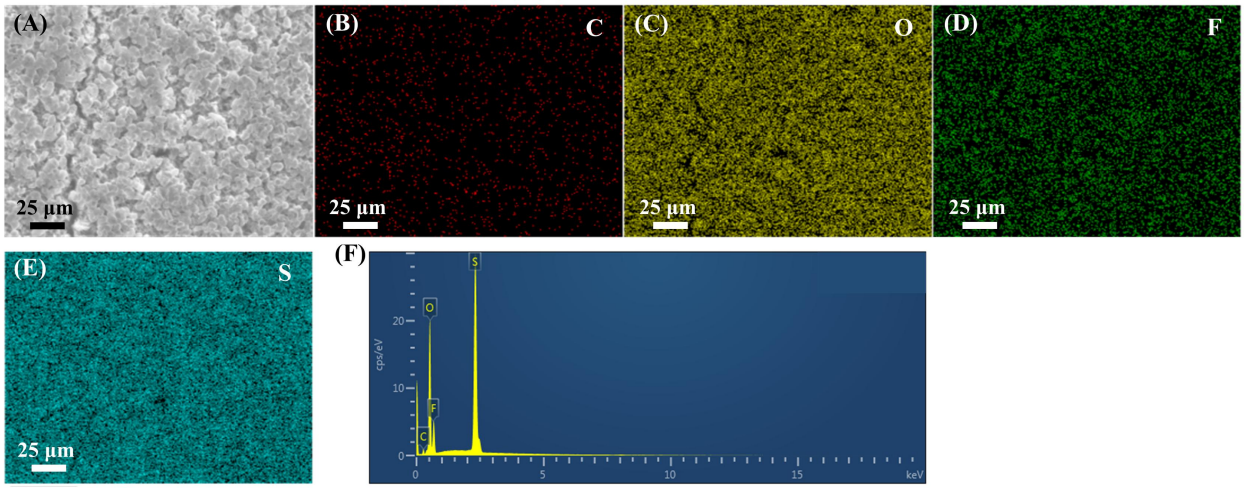

Supplementary Figure 10. (A) SEM image and (B-F) corresponding element analysis of Li metal anode from the MXene@PP-based Li-S cell.

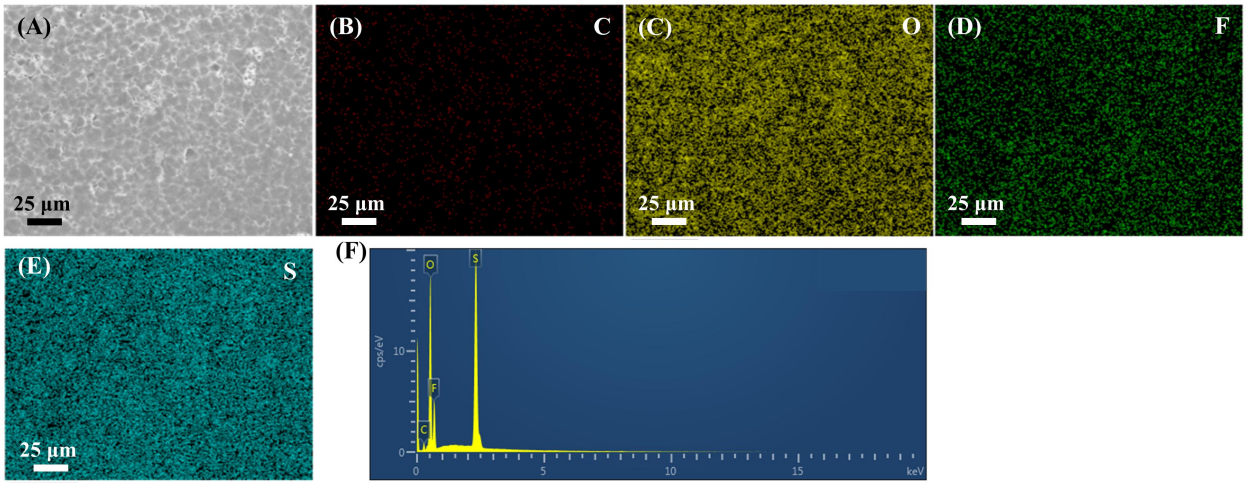

Supplementary Figure 11. (A) SEM image and (B-F) corresponding element analysis of Li metal anode from the ZIF-L/MXene@PP-based Li-S cell.

Supplementary Table 1. Electrochemical performance comparisons of the ZIF-L/MXene-PP separator with other functional separators in recent literature.

Interlayer material	Sulfur loading (mg cm^{-2})	Interlayer loading (mg cm^{-2})	Interlayer thickness (μm)	Current density (C)	Specific capacity (mAh g^{-1})	Reference
ZIF-L/MXene	**1.2-1.5** **~ 4.1**	**0.13**	**~ 3.3**	**2.0** **0.1**	**710.2** **990.6**	**This work**
ZnS/MXene	0.8-1.2 5.2	0.3-0.4	~ 5.0	2.0 0.2	798.9 1010.5	[1]
Co_2B@MXene	1.2-1.5 5.1	/	14.7	2.0 0.2	775 5.2 mAh cm^{-2}	[2]
OMC-g-MXene	~ 1.2 7.08	/	/	2.0 0.1	744 4.5 mAh cm^{-2}	[3]
DE/MXene	1.0	0.2	9.0	2.0	703	[4]
PM (0.4 M)-CNT	~ 0.9 2.42	0.16	~ 4	2.0 0.2	677 998	[5]
$Ti_3C_2T_x$/Ni-Co MOF	1.5 5.8	0.2	4.5	2.0 0.1	660 730	[6]
I-MXene	1.0 6.5	/	10	2.0 0.2	655 889	[7]
HPCA-TO	0.8	0.4	/	2.0	635	[8]
DNA-CNT/MXene	1.0	0.1	~ 0.575	2.0	588	[9]
IL-MoS_2/MX	1.2-1.5	0.08	1.0	1.0	745.4	[10]

References

[1] C. Wei, B. Xi, P. Wang, et al., In situ anchoring ultrafine ZnS nanodots on 2D MXene nanosheets for accelerating polysulfide redox and regulating Li plating, *Adv Mater* 2023;35:2303780. [DOI: 10.1002/adma.202303780].

[2] B. Guan, X. Sun, Y. Zhang, et al., The discovery of interfacial electronic interaction within cobalt boride@MXene for high performance lithium-sulfur batteries, *Chin Chem Lett* 2021;32:2249-2253. [DOI: 10.1016/j.cclet.2020.12.051].

[3] X. Li, Q. Guan, Z. Zhuang, et al., Ordered mesoporous carbon grafted MXene catalytic heterostructure as Li-ion kinetic pump toward high-efficient sulfur/sulfide conversions for Li–S battery, *ACS Nano* 2023;17:1653-1662. [DOI: 10.1021/acsnano.2c11663].

[4] Z. Fan, C. Zhang, W. Hua, et al., Enhanced chemical trapping and catalytic conversion of polysulfides by diatomite/MXene hybrid interlayer for stable Li-S batteries, *J Energy Chem* 2021;62:590-598. [DOI: 10.1016/j.jechem.2021.04.038].

[5] D. Xiong, S. Huang, D. Fang, et al., Porosity engineering of MXene membrane towards polysulfide inhibition and fast lithium ion transportation for lithium–sulfur batteries, *Small* 2021;17:2007442. [DOI: 10.1002/smll.202007442].

[6] Y. Ren, Q. Zhai, B. Wang, et al., Synergistic adsorption-electrocatalysis of 2D/2D heterostructure toward high performance Li-S batteries, *Chem Eng J* 2022;439:135535. [DOI: 10.1016/j.cej.2022.135535].

[7] W. Yu, S. Ma, M. He, et al., Immobilization and kinetic acceleration of lithium polysulfides by iodine-doped MXene nanosheets in lithium–sulfur batteries, *J Phys Chem C* 2022;126:10986-10994. [DOI: 10.1021/acs.jpcc.2c02689].

[8] C. Shi, J. Huang, Y. Tang, et al., A hierarchical porous carbon aerogel embedded with small-sized TiO_2 nanoparticles for high-performance Li–S batteries, *Carbon* 2023;202:59-65. [DOI: 10.1016/j.carbon.2022.09.086].

[9] Y. Li, M. Li, Y.-C. Zhu, et al., Polysulfide-inhibiting, thermotolerant and nonflammable separators enabled by DNA co-assembled CNT/MXene networks for stable high-safety Li–S batteries, *Compos B Eng* 2023;251:110465. [DOI: 10.1016/j.compositesb.2022.110465].

[10] F. Xie, C. Xu, Y. Song, Q. Liang, J. Ji, S. Wang, 2D-2D heterostructure of ionic liquid-exfoliated MoS_2/MXene as lithium polysulfide barrier for Li-S batteries, *J Colloid Interface Sci* 2023;636:528-536. [DOI: 10.1016/j.jcis.2023.01.031].